Equilibrium and dynamic design principles for binding molecules engineered for reagentless biosensors

Published in final edited form as:
Anal Biochem. 2014 September 1; 0: 9–15. doi:10.1016/j.ab.2014.04.036.

EQUILIBRIUM AND DYNAMIC DESIGN PRINCIPLES FOR BINDING MOLECULES ENGINEERED FOR REAGENTLESS BIOSENSORS

Seymour de Picciotto[1], **Barbara Imperiali**[2,3], **Linda G. Griffith**[1,4], and **K. Dane Wittrup**[1,4,5,**]

[1]Department of Biological Engineering, Massachusetts Institute of Technology

[2]Department of Biology, Massachusetts Institute of Technology

[3]Department of Chemistry, Massachusetts Institute of Technology

[4]Koch Institute for Integrative Cancer Research

[5]Department of Chemical Engineering, Massachusetts Institute of Technology

Abstract

Reagentless biosensors rely on the interaction of a binding partner and its target to generate a change in fluorescent signal using an environment sensitive fluorophore or Förster Resonance Energy Transfer. Binding affinity can exert a significant influence on both the equilibrium and the dynamic response characteristics of such a biosensor. We here develop a kinetic model for the dynamic performance of a reagentless biosensor. Using a sinusoidal signal for ligand concentration, our findings suggest that it is optimal to use a binding moiety whose equilibrium dissociation constant matches that of the average predicted input signal, while maximizing both the association rate constant and the dissociation rate constant at the necessary ratio to create the desired equilibrium constant. Although practical limitations constrain the attainment of these objectives, the derivation of these design principles provides guidance for improved reagentless biosensor performance and metrics for quality standards in the development of biosensors. These concepts are broadly relevant to reagentless biosensor modalities.

Keywords

Reagentless biosensor; dynamic analysis; antibody immunoassay; detection

**Address correspondence to: K. Dane Wittrup, Building 76-261, 500 Main Street, Cambridge, MA 02139, Phone: 617-253-4578, wittrup@MIT.EDU.

1. Introduction

The field of biosensors has seen in the last decade a multitude of new approaches for the application of reagentless sensors. The overall strategy is the combination of a recognition unit and a signal-transducing unit into one molecular entity. The most commonly-used signal is change in sensor fluorescence, arising either from Fluorescence Resonance Energy Transfer (FRET) or from solvatochromism. FRET was first described over half a century ago, and its application in biology has grown with design and implementation of myriad biosensors (reviewed in [1]). Solvatochromism is a more recent development, but is becoming more widely used as new scaffolds (affinity molecules) and dyes (environmentally-sensitive fluorophores) are developed and become available (reviewed in [2]). Several groups have successfully developed solvatochromic-based biosensors using DNA aptamers [3–5], native protein receptors[6,7], peptides[8,9] or engineered binders using protein scaffolds[10–15]. However, to our knowledge, none of these groups have purposely engineered binders with affinities specified for optimal performance as a sensor, relying instead on previously-described proteins. Selecting an existing binder with an affinity above the detection threshold is likely an adequate approach for categorical detection of the presence or absence of an analyte. However in a complex biological system, analyte concentrations may vary rapidly on the timescale of seconds to minutes. For dynamic measurement of time-varying analyte levels, the biophysical characteristics of the binding event can significantly impact biosensor accuracy and sensitivity. Given the availability of directed evolution protein engineering methodology to create binding molecules of almost arbitrary affinity and widely varying association and dissociation rates[16,17], these variables are available degrees of freedom for improvement of biosensor performance. Recently Haugh developed a reaction-diffusion model to investigate biosensor signal interpretation in live cell imaging, with an emphasis on capturing intracellular and membrane-localized phenomena[18]. This analysis resulted in the identification of an important trade-off between robust signal and perturbation of the biological system or signal saturation. Here, we perform a theoretical analysis of biosensor dynamics, delineating time and length scales important in observation of intracellular as well as extracellular phenomena (*e.g.* detecting autocrine loops). Using a sinusoidal signal as an input ligand concentration, as biological signal do vary, we present new important considerations for the appropriate implementation of a biosensor. Further, we propose metrics for quality standards in the development of biosensors by direct comparison between the input signal and measured signal and, thereby derive design criteria for improved performance.

2. Model formulation

The system consists of three state variables: the concentrations of ligand (L), unbound sensor (S_F) and bound sensor (S_B). By virtue of mass balance, the sum of the concentration of unbound and bound sensor is always equal to the total sensor concentration constant (S_{Tot}). A linear correlation between bound sensor and the output signal intensity is assumed. The two rate constants governing this process are the association (k_{on}) and the dissociation (k_{off}) rate constant.

The mathematical description of this interaction, a reversible bimolecular reaction, is well documented from the perspective of dynamic steady state equilibrium; however, it has generally been investigated in an environment of constant ligand concentration[19–21]. To determine the optimal design criteria in a dynamic system where the input (i.e., L) is time-varying, we apply a frequency response approach by sinusoidally varying the analyte input, L, and characterizing the dynamic fluorescence intensity response of the sensor, which is proportional to the concentration of bound sensor S_B. A range of physiological behaviors can be modeled by systematic variation of the mean (L_0), amplitude (A_L) and period (T) of the time-variant ligand concentration. With these parameter definitions, the input function L is defined as:

$$[\mathrm{L}]=\mathrm{L}_0+\mathrm{A}_\mathrm{L}\sin(2\pi/\mathrm{T}\,t) \quad (1)$$

To score a given set of design parameters of a sensor, we choose three signal properties: mean signal intensity (M), normalized amplitude (A) and phase delay (Φ), as defined in equations 2–4.

$$\mathrm{M}=({\mathrm{S}_\mathrm{B}}^{\mathrm{max,eq}}+{\mathrm{S}_\mathrm{B}}^{\mathrm{min,eq}})/2\mathrm{S}_{\mathrm{Tot}} \quad (2)$$

$$\mathrm{A}=({\mathrm{S}_\mathrm{B}}^{\mathrm{max,eq}}-{\mathrm{S}_\mathrm{B}}^{\mathrm{min,eq}})/\mathrm{S}_{\mathrm{Tot}} \quad (3)$$

$$\Phi=(\mathrm{t}(\mathrm{S}_\mathrm{B}={\mathrm{S}_\mathrm{B}}^{\mathrm{max,eq}})-\mathrm{t}(\mathrm{S}_\mathrm{B}={\mathrm{S}_\mathrm{B}}^{\mathrm{min,eq}}))/\mathrm{T} \quad (4)$$

We assume that the system is reaction limited. Indeed the Damkohler number, defined as the ratio between the characteristic time for diffusion and that of reaction (complex formation in this context, see equation 5), will be much smaller than 1 for all relevant k_{on}, k_{off}, ligand concentration ([L]), diffusion coefficient (D) so long as the distance (r_b) over which the measurement must be spatially resolved is less than 1 micron (see Figure S1).

$$\mathrm{Damkohler}\#=\tau_{\mathrm{diff}}/\tau_{\mathrm{rxn}}=({\mathrm{r}_\mathrm{b}}^2/\mathrm{D})/(\mathrm{k}_{\mathrm{on}}[\mathrm{L}]+\mathrm{k}_{\mathrm{off}})^{-1}) \quad (5)$$

The described system is now fully governed by the three differential equations:

$$\mathrm{d}[\mathrm{L}]/\mathrm{dt}=2\pi/\mathrm{T}\,\mathrm{A}_\mathrm{L}\cos(2/\mathrm{T}\,t)-\mathrm{k}_{\mathrm{on}}[\mathrm{L}][\mathrm{S}_\mathrm{F}]+\mathrm{k}_{\mathrm{off}}[\mathrm{S}_\mathrm{B}] \quad (6)$$

$$\mathrm{d}[\mathrm{S}_\mathrm{F}]/\mathrm{dt}=-\mathrm{k}_{\mathrm{on}}[\mathrm{L}][\mathrm{S}_\mathrm{F}]+\mathrm{k}_{\mathrm{off}}[\mathrm{S}_\mathrm{B}] \quad (7)$$

$$\mathrm{d}[\mathrm{S}_\mathrm{B}]/\mathrm{dt}=+\mathrm{k}_{\mathrm{on}}[\mathrm{L}][\mathrm{S}_\mathrm{F}]-\mathrm{k}_{\mathrm{off}}[\mathrm{S}_\mathrm{B}] \quad (8)$$

To simplify this system further, we assume that the ligand is in excess. Of course, as shown in the analysis by Haugh[18], this is a constraint that must be calculated for any real system

since this assumption can often break down. Systematic use of a sensor concentration of one twentieth that of the minimum ligand signal guarantees excess ligand concentration. By substituting equation 1 into 8, and using conservation of mass for the sensor species, we obtain the 1-D governing equation:

$$d[S_B]/dt = k_{on}(S_{Tot} - S_B)(L_0 + A_L \sin(2\pi/T\, t)) - k_{off}[S_B] \quad (9)$$

A convenient analytical solution to this system is not available. Therefore, we solved this equation for a variety of parameter conditions by numerical Euler integration (performed in MatLab). The results are shown in the next section.

3. Results

Dynamic consideration reveals the crucial importance of kinetic rates optimization

Intuitively, a sensor that has a very high affinity for its ligand might be expected to perform as a weak dynamic sensor since the characteristic time for complex dissociation would likely be much greater than the period of the signal. Relevant input signal conditions depend greatly on the system under study. In Figure 1 we show approximate concentrations and time scales for concentration variation for various classes of biological events. Many physiological processes result in great variation of analyte concentration such as cell-cycle related proteins, signaling cascades, immune response activation among many others. Mathematically, the sinusoidal function is a benchmark for representing time-variant signals. For example the well-known Bode plot uses a sinusoidal signal to characterize a system's frequency response[22]. We first investigated how output signal differs with varying the dissociation rate constant (k_{off}). As an initial input signal, we chose a mean ligand concentration of 3 nM with sinusoidal oscillation between 1 and 5 nM with a period of 100 minutes. This signal is shown as a solid gray curve on Figure 2A. In black are shown four different sensors with varying k_{off} but identical association rate constant ($k_{on} = 10^5$ $M^{-1}s^{-1}$). In this first approach, we show the signal for the first 4 periods (400 minutes). An initial condition corresponding to $S_B = 0$ was chosen for the analysis depicted in Figure 2A, hence an initial transient in signal response is observed. The signals progress toward their dynamic steady state, where higher signal intensities are reached with decreasing k_{off} as expected given the equation for complex concentration under the pseudo-first order approximation (see equation 10).

$$[S_B] = S_{Tot}\, L_0/(L_0 + k_{off}/k_{on}) \quad (10)$$

This transient behavior is followed by a dynamic steady state characterized by a constant value of the mean signal. The equilibrium half time ($t_{1/2}$) is defined as:

$$\tau_{1/2} = \ln(2)/(k_{on}\, L_0 + k_{off}) \quad (11)$$

The periodic signal is assumed stable for $t > 100*\tau_{1/2}$, when the transient conditions would have decayed substantially. In the subsequent analysis, we report signals when $t > 100*\tau_{1/2}$.

We therefore plotted the amplitude and mean signal value for the signals in Figure 2B as a function of k_{off}. In both the transient and dynamic steady state regimes, the mean signal value increases with decreasing k_{off}. The oscillation amplitude appears very small for both extreme k_{off} values. However, there is an optimum at intermediate values as seen when the amplitude and mean signal value are plotted as a function of k_{off} (Fig 2B). Interestingly, the optimum k_{off} value for this particular example is a physically realistic rate of $2*10^{-4}$ s^{-1}.

Varying input characteristics

We next investigated how this optimum region behaves with different input signal characteristics across 3 orders of magnitude of mean ligand concentration for various sensor properties (k_{on} and k_{off} values) and a constant oscillation period of T = 100 min (Figure 3). The amplitude was also held constant at $A_L = 2/3*L_0$ (see Eq. 1). Recognizing that any particular sensor will be most sensitive over about a 10-fold concentration range, we divided the analysis into 3 concentration regimes representing anticipated physiological values of interest for oscillation (0.1–0.5 nM; 1–5 nM; 10–50 nM). Within each regime, we created heat maps to reflect normalized values of mean signal, mean amplitude, and phase shift for combinations of k_{off} and k_{on} spanning 6 orders of magnitude (Figure 3).

The general features of the heat map are illustrated by Figure 3a, which depicts the mean output signal intensity (% max signal) for oscillation of L in the low concentration regime (0.1–0.5 nM). Regions in white at the bottom left indicate a high mean signal and are associated with the regime of tightest equilibrium binding affinity ($K_D = k_{off}/k_{on}$); i.e., the regime where the receptor is saturated so that it is insensitive to variations in k_{on} and k_{off}. The diagonal at which the normalized mean signal intensity is 50% of the maximum corresponds to values where $K_D = L_0$. The position of this diagonal is naturally shifted upward as the mean ligand concentration is increased 10-fold to 3 nM (Figure 3e) and 100-fold to 30 nM (Figure 3i). By this criterion alone, the desire for robust signal detection would favor biosensors that have $K_D < L_0$, with greatest sensitivity for concentration discrimination (versus just threshold concentration detection) in the range $K_D \sim L0$. However, consideration of dynamic response introduces additional constraints as discussed below.

Despite strong mean signal intensity, the highest affinity binders, with k_{on} and k_{off} represented on the bottom right of each panel of Figure 3a, e, and i, are insensitive to time varying concentrations of the ligand. This phenomenon can be appreciated by examining the amplitude of the output signal as defined in Equation (3) and plotted as heat maps in Figure 3b (L variation of 0.1–0.5 nM), f (L variation of 1–5 nM), and j (L variation of 10–50 nM). The region of greatest output signal amplitude is shown in white and is obtained for fast kinetic rate constants. Fast association rate constants mean that the biosensor is quickly able to capture ligand and therefore rapidly report the signal, while fast dissociation is crucial to adapt the variations in ligand concentration. This optimum area lines up again with an equilibrium dissociation constant $K_D = L_0$, however, fast kinetic rates are crucial to prevent the binding dynamics from obscuring the input (ligand oscillation) dynamics. As the mean ligand concentration rises from values in Figure 3b, to those in 3f and j the abundance of

ligand makes it easier for the sensor to capture and report the signal. This is illustrated by the shift to the left of the optimal region.

Figure 3c shows the phase shift, which is a measure of the delay in signal reporting. Here the favored regions are those of low shift, shown in white. It can be seen that again faster kinetic rates are beneficial in reporting accurately the input signal. This optimal region expands to slower kinetics as L_0 increases from Figure 3c, 3g to 3k.

In order to evaluate these three criteria simultaneously, we first define for illustrative purposes an arbitrary design threshold for each: M > 20%, A > 10% and $\Phi < 0.1$. We then plotted on the 4th column of Figure 3 the region of k_{on} and k_{off} where all criteria are satisfied. We observe that the criteria are easier to meet for conditions of high mean ligand concentration. For the example with the lowest ligand concentration (oscillating between 0.1 and 0.5nM), only a narrow range of rate constant combinations results in adequate performance by the chosen criteria. Therefore, depending on the ligand conditions, it may be necessary to sacrifice some characteristic of the output.

In Figure 3 we have shown the dependency of the kinetic rate constants on the location of optimal regions for the three different biosensor design criteria and investigated how the sensors characteristics are affected for different mean ligand concentrations. The same approach can be undertaken by varying the other two parameters – in ranges that are biologically relevant – of the input signal (period and amplitude); we have summarized the effects on the position of optimal $<k_{on}, k_{off}>$ region in Table 1. The output mean signal is insensitive to changes in input frequency or amplitude. However, for extreme conditions the changes in concentration occur very rapidly and the effective mean concentration rises. This phenomenon is present only for dynamics that are orders of magnitude faster than any biological process. Finally, it is interesting to note that increase in the input amplitude has no effect on the position of the optimum.

Single sensor analysis

So far we have been exploring how a variety of sensors perform for a circumscribed set of input signal conditions. We next analyzed how a set of 3 individual sensors, with combinations of properties that span the spectrum of physically possible values, performs in a variety of different input conditions. To do so, we use a Bode diagram representation since it is the canonical approach for representing dynamic systems responses. Oscillation cycle times spanning the range 10 min – 40 hr (frequencies of 3×10^{-6} to 3×10^{-3} Hz) were examined as it encompasses a great range of physiologically relevant systems (Figure 1). For a signal oscillating between 1 and 5 nM and a sensor concentration of 0.05nM, we have represented the normalized amplitude, phase shift and mean signal in Figure 4 for three different sensors over this: In solid black we have represented a tight binder ($k_{on} = 10^6$ $M^{-1}s^{-1}$, $k_{off} = 10^{-6}$ s^{-1}), in dashed black a utopian binder ($k_{on} = 10^8$ $M^{-1}s^{-1}$, $k_{off} = 10^{-1}$ s^{-1}) with ideal characteristics but physically non feasible, and in dotted black a feasible binder ($k_{on} = 10^6$ $M^{-1}s^{-1}$, $k_{off} = 3*10^{-3}$ s^{-1}).

Without a dynamic analysis of this system, the tight binder would likely be chosen as the most adequate sensor because of its high mean signal (fractional saturation). However, the

normalized amplitude of this sensor is null for the relevant input system frequencies. The utopian sensor performs well in a variety of conditions, the phase shift is less than 10% for signal frequencies < 0.01 s^{-1}. However, the k_{on} of this sensor, 10^8 $M^{-1}s^{-1}$, is physically not achievable in general; a more typical protein/protein k_{on} =10^5–10^6 $M^{-1}s^{-1}$. In the dotted black line is represented a feasible sensor, named so because it performs well in wide range of frequencies and it is technically feasible. The normalized mean signal for the feasible sensor increases with faster frequencies as the biosensor inaccurately reflects a higher signal.

4. Discussion

We have shown that there exists an optimal combination of the design parameters k_{on} and k_{off} for a reagentless biosensor and that these vary depending on the nature of the signal. What our results indicate is that the careful determination of binding kinetics is crucial for successful application of biosensors. As a general rule, the K_D of the interaction must match that of the expected mean ligand concentration to ensure greatest sensitivity. Biosensors with a K_D lower that the mean ligand concentration will yield a binary output. Faster association and dissociation rate constants combinations provide greater correlation to the input signal. Therefore, efforts to increase both k_{on} and k_{off} while maintain a K_D near the expected ligand concentration will generally improve dynamic response time while maintaining sensitivity.

While the presence of an optimal k_{off}, k_{on} combination may exist for a given input signal, these rate constants may not be either physically relevant or in the range of what can be engineered. The dissociation rate constant is very amenable to changes and most library selection strategies rely on optimizing this parameter. For the association rate constant, the scenario is quite different: two molecules come together by diffusion which is governed by Brownian motion. Smoluchowski calculated that if proteins were smooth spheres and they formed a complex every time they would collide, the association rate dictated by Brownian motion would thus be $7*10^9$ $M^{-1}s^{-1}$. However, complex formation requires stringent orientation constraints and the observed rate of protein-protein complex formation is 10^5–10^6 $M^{-1}s^{-1}$ [23,24]. Nevertheless, some outliers for protein-protein and DNA-protein have been identified with association rates up to 10^9 $M^{-1}s^{-1}$ [25–28] due to favorable electrostatic interactions, and very slow association rates (10^3 $M^{-1}s^{-1}$) due to high energy barriers to complex formation[29]. Within the gray box of Figure 3a are the regions considered generally accessible to protein engineering. A large range of k_{on}, k_{off} couples with high performance are well outside the range of physical possibilities.

While the optimum set of constants cannot always be achieved, there are some alternatives that can be used. Renard & Bedouelle successfully demonstrated the use of three sensors with various affinities against lysozyme in combination in order to titrate lysozyme concentration over a three log range[30]. Another group also demonstrated the possibility of narrowing the titration range using a depletion strategy[31]. Moreover a combination of sensors with different output signal characteristic can be beneficial also for dynamic scenarios. We exemplify here the possibility of using a combination of different sensors at equimolar concentrations each with different dissociation rate constants to form a more robust sensing system as illustrated in Figure 5. The three sensors have an association rate

constant of 10^5 $M^{-1}s^{-1}$ and equilibrium dissociation constants of 100, 10 and 1 nM. Suppose for a given application that the tightest binder offers a more than satisfactory mean signal intensity but suffers from profound signal delays, not acceptable for that application. The intensity of the signal can only be correlated to a concentration of target antigen if appropriate calibrations controls have been established. While, in general, greater signal intensities are preferred as they are facilitate detection and have lower signal to noise ratios. In some cases, it is possible to sacrifice some of the signal intensity in order to improve other characteristics of the signal. Indeed, the weaker binders do offer better signal correlation as indicated by the lower phase shift, but the signal intensity may be too weak. By combining these sensors together, one obtains a signal profile that now offers improved time correlation and satisfactory mean signal intensity. The ratios and properties of these sensors can be fine tuned to obtain the desired output signal properties. This approach is advantageous as it allows manipulation of the sensor signal properties without any additional engineering, given the condition of having at least two sensors. The Matlab code provided online allows the reader to quickly assess any desired combinations.

While this model can be applied to any particular ligand concentration and variation dynamics, we have here often focused on the low nanomolar concentration range. This concentration range was motivated by the ErbB extracellular signaling network. The ErbB receptor family is activated by growth factor shedding in an autocrine or paracrine manner. Previous mathematical modeling based on experimental evidence by the Lauffenburger and Wiley groups has allowed the determination of the effective ligand concentration at the cell surface[32–34]. By controlling ligand production, shedding and receptor levels, Dewitt et al. were able to determine a direct relationship between ligand shedding rate and effective concentration, shown to be in the 1–10 nM range[32]. Hence, we have chosen the range of 1–5 nM for most of our demonstration. As shown in Figure 1, there is a great variety in the concentration and dynamics of physiologically relevant molecules. Our model strongly indicates that careful optimization of a biosensor is critical for its appropriate deployment to investigate the biological system of interest.

Previous biosensor modeling efforts have ranged from finite element methods for microelectromechanical systems[35], to partial differential equation systems of enzymatic reactions[36]. In the field of reagentless biosensors, Haugh developed a reaction-diffusion model and showed the importance of binding parameter optimization to prevent signal saturation or system perturbation[18]. Our analysis distinguishes itself by revealing that kinetic rate constants are crucial to the proper identification of signal fluctuations. We have provided guidelines for the optimization of these parameters for a desired application. Furthermore, from this dynamic analysis, we derived metrics which we suggest should become standard for the characterization of biosensors.

Often biosensors detection mechanisms rely on tethering receptor onto microchips. In these systems, convection and diffusion are essential properties that were not investigated in our model since they were assumed negligible. Squires et al., investigated design constraints imposed by transport in surface-based biosensors[37]. Through finite element methods, they discussed the time scales and collection rates for these systems as a function of the channel dimensions, flow rate, ligand diffusion and binding kinetics. Although not discussed in their

publication, faster kinetics for the ligand-receptor interaction would likely improve the correlation between the input and output signal in these systems as well. Furthermore, they highlight the importance of tethered receptor density as higher density would allow lower detection limits and also increased signal to noise ratio. Thus, we suggest that reagentless biosensors could be clustered on the surface of beads. This would greatly improve the signal to noise ratio in fluorescent microscopy read-out. But as underlined in the model published by Squires et al., increased binder density correlates with greater depletion effects which ultimately could have adverse local effect on the physiology of the system.

To our knowledge, we present here the first analysis of a sensor system for kinetic rate constants optimization under dynamic conditions. Furthermore we have specifically identified three criteria for scoring the applicability of reagentless biosensors: mean, amplitude and phase shift. Based on the analysis of these criteria, we have presented here the limitations and trade-offs in the design of biosensors. While several reviews have been published for the design principles of reagentless sensors[1,38], they fail to acknowledge the importance of sensor-ligand kinetic binding parameters optimization for their particular application. Only through a dynamic analysis, as presented here, can the importance of the kinetic constants be highlighted.

The results described here hold true if the sensor concentration is appropriate to guarantee no ligand depletion. Ligand depletion would not only affect the founding assumption of this model but also severely perturb the biological sample to be studied. In this context, this model can significantly help scientists in choosing the adequate binding parameters of their sensor and the biological system to be studied to maximize their efficacy.

Supplementary Material

Refer to Web version on PubMed Central for supplementary material.

Acknowledgments

The authors would like to thank Dr. Alan Wells and Dr. Neda Bagheri for helpful discussions. This work was supported by the Integrative Cancer Biology Program (ICBP 1 U54 CA112967) and by NIH R01 EB 010246.

References

1. Lemke EA, Schultz C. Principles for designing fluorescent sensors and reporters. Nat Chem Biol. 2011; 7:480–3. [PubMed: 21769088]
2. Loving GS, Sainlos M, Imperiali B. Monitoring protein interactions and dynamics with solvatochromic fluorophores. Trends Biotechnol. 2010; 28:73–83. [PubMed: 19962774]
3. Wang HQ, Wu Z, Tang LJ, Yu RQ, Jiang JH. Fluorescence protection assay: a novel homogeneous assay platform toward development of aptamer sensors for protein detection. Nucleic Acids Res. 2011; 39:e122. [PubMed: 21742759]
4. Zhao W, Schafer S, Choi J, Yamanaka YJ, Lombardi ML, Bose S, et al. Cell-surface sensors for real-time probing of cellular environments. Nat Nanotechnol. 2011; 6:524–531. [PubMed: 21765401]
5. Paige JS, Nguyen-Duc T, Song W, Jaffrey SR. Fluorescence imaging of cellular metabolites with RNA. Science. 2012; 335:1194. [PubMed: 22403384]

6. Loving G, Imperiali B. A versatile amino acid analogue of the solvatochromic fluorophore 4-N,N-dimethylamino-1,8-naphthalimide: a powerful tool for the study of dynamic protein interactions. J Am Chem Soc. 2008; 130:13630–8. [PubMed: 18808123]
7. Goguen BN, Loving GS, Imperiali B. Development of a fluorogenic sensor for activated Cdc42. Bioorg Med Chem Lett. 2011; 21:2–5.
8. Choulier L, Shvadchak VV, Naidoo A, Klymchenko AS, Mély Y, Altschuh D. A peptide-based fluorescent ratiometric sensor for quantitative detection of proteins. Anal Biochem. 2010; 401:188–95. [PubMed: 20188691]
9. Pazos E, Pérez M, Gutiérrez-de-Terán H, Orzáez M, Guevara T, Mascareñas JL, et al. Rational design of a cyclin A fluorescent peptide sensor. Org Biomol Chem. 2011; 9:7629–32. [PubMed: 21863156]
10. Renard M, Belkadi L, Hugo N, England P, Altschuh D, Bedouelle H. Knowledge-based design of reagentless fluorescent biosensors from recombinant antibodies. J Mol Biol. 2002; 318:429–42. [PubMed: 12051849]
11. Miranda FF, Brient-Litzler E, Zidane N, Pecorari F, Bedouelle H. Reagentless fluorescent biosensors from artificial families of antigen binding proteins. Biosens Bioelectron. 2011; 26:4184–90. [PubMed: 21565483]
12. Gulyani A, Vitriol E, Allen R, Wu J, Gremyachinskiy D, Lewis S, et al. A biosensor generated via high-throughput screening quantifies cell edge Src dynamics. Nat Chem Biol. 2011; 7:437–44. [PubMed: 21666688]
13. Abe R, Ohashi H, Iijima I, Ihara M, Takagi H, Hohsaka T, et al. “Quenchbodies”: Quench-Based Antibody Probes That Show Antigen-Dependent Fluorescence. J Am Chem Soc. 2011; 133:17386–17394. [PubMed: 21977983]
14. Kummer L, Hsu CW, Dagliyan O, Macnevin C, Kaufholz M, Zimmermann B, et al. Knowledge-Based Design of a Biosensor to Quantify Localized ERK Activation in Living Cells. Chem Biol. 2013; 20:847–56. [PubMed: 23790495]
15. Brient-Litzler E, Plückthun A, Bedouelle H. Knowledge-based design of reagentless fluorescent biosensors from a designed ankyrin repeat protein. Protein Eng Des Sel. 2010; 23:229–41. [PubMed: 19945965]
16. Gai SA, Wittrup KD. Yeast surface display for protein engineering and characterization. Curr Opin Struct Biol. 2007; 17:467–73. [PubMed: 17870469]
17. Pepper LR, Parthasarathy R, Robbins GP, Dang Da Hammer NN, Boder ET. Isolation of αL I domain mutants mediating firm cell adhesion using a novel flow-based sorting method. Protein Eng Des Sel. 2013; 8:515–521.
18. Haugh JM. Live-cell fluorescence microscopy with molecular biosensors: what are we really measuring? Biophys J. 2012; 102:2003–11. [PubMed: 22824263]
19. Lauffenburger, DA.; Linderman, J. Receptors: models for binding, trafficking, and signaling. Oxford University Press; New York, NY: 1993.
20. Connors, KA. Chemical kinetics: the study of reaction rates in solution. John Wiley & Sons; 1990.
21. Chen, L.; Wang, R.; Li, C.; Aihara, K. Modeling Biomolecular Networks in Cells: Structures and Dynamics. Springer; New York: 2010.
22. Bode, HW. Network analysis and feedback amplifier design. Van Nostrand; 1945.
23. Northrup SH, Erickson HP. Kinetics of protein-protein association explained by Brownian dynamics computer simulation. Proc Natl Acad Sci U S A. 1992; 89:3338–42. [PubMed: 1565624]
24. Marvin JS, Lowman HB. Redesigning an antibody fragment for faster association with its antigen. Biochemistry. 2003; 42:7077–83. [PubMed: 12795603]
25. Schreiber G, Fersht AR. Interaction of barnase with its polypeptide inhibitor barstar studied by protein engineering. Biochemistry. 1993; 32:5145–50. [PubMed: 8494892]
26. Stone SR, Hofsteenge J. Kinetics of the inhibition of thrombin by hirudin. Biochemistry. 1986; 25:4622–8. [PubMed: 3768302]
27. Kirchhoff PD, Quinn DM, Mccammon JA, Taylor P. Electrostatic Influence on the Kinetics of Ligand Binding to. 1997; 272:23265–23277.

28. Halford SE. An end to 40 years of mistakes in DNA-protein association kinetics? Biochem Soc Trans. 2009; 37:343–8. [PubMed: 19290859]

29. Li Y, Lipschultz CA, Mohan S, Smith-Gill SJ. Mutations of an epitope hot-spot residue alter rate limiting steps of antigen-antibody protein-protein associations. Biochemistry. 2001; 40:2011–22. [PubMed: 11329268]

30. Renard M, Bedouelle H. Improving the Sensitivity and Dynamic Range of Reagentless Fluorescent Immunosensors by Knowledge-Based Design †. Society. 2004:15453–15462.

31. Vallée-Bélisle A, Ricci F, Plaxco KW. Engineering Biosensors with Extended, Narrowed, or Abirtrarily Edited Dynamic Range. J Am Chem Soc. 2012; 134:2876–2879. [PubMed: 22239688]

32. DeWitt AE, Dong JY, Wiley HS, Lauffenburger DA. Quantitative analysis of the EGF receptor autocrine system reveals cryptic regulation of cell response by ligand capture. J Cell Sci. 2001; 114:2301–13. [PubMed: 11493669]

33. Shvartsman SY, Wiley HS, Deen WM, Lauffenburger DA. Spatial Range of Autocrine Signaling: Modeling and. Biophys J. 2001; 81:1854–1867. [PubMed: 11566760]

34. Dewitt A, Iida T, Lam H, Hill V, Wiley H, Lauffenburger D. Affinity Regulates Spatial Range of EGF Receptor Autocrine Ligand Binding. Dev Biol. 2002; 250:305–316. [PubMed: 12376105]

35. Lim YH, Varadan VV, Varadan VK. Finite-element modeling of the transient response of MEMS sensors. Smart Mater Struct. 1997; 6:53–61.

36. Schulmeister T, Rose J, Scheller F. Mathematical modelling of exponential amplification in membrane-based enzyme sensors. Biosens Bioelectron. 1997; 12:1021–1030.

37. Squires TM, Messinger RJ, Manalis SR. Making it stick: convection, reaction and diffusion in surface-based biosensors. Nat Biotechnol. 2008; 26:417–26. [PubMed: 18392027]

38. Tainaka K, Sakaguchi R, Hayashi H, Nakano S, Liew FF, Morii T. Design strategies of fluorescent biosensors based on biological macromolecular receptors. Sensors (Basel). 2010; 10:1355–76. [PubMed: 22205872]

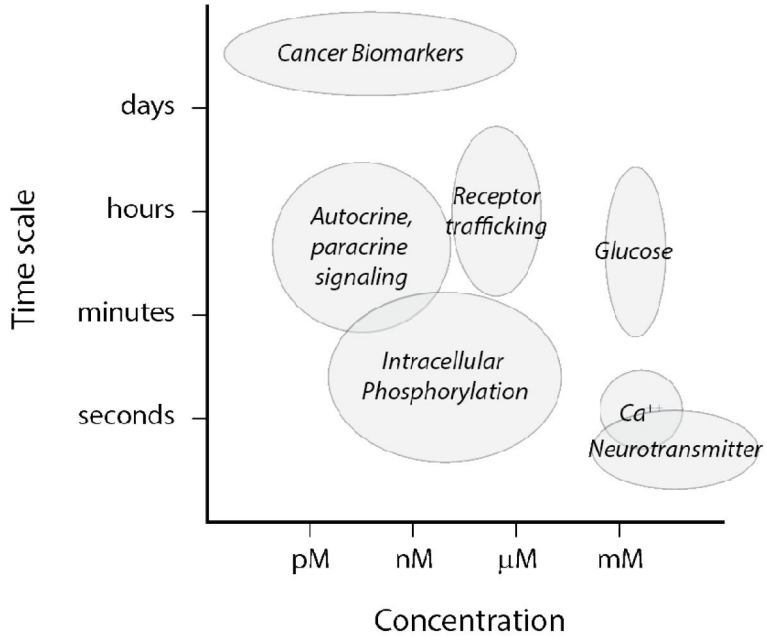

Figure 1.

Various biologically relevant molecules and processes are depicted in this Figure. Typical mean concentration is shown on the horizontal axis ranging from picomolar (pM) to millimolar (mM) against expected time scales for variation in the ligand concentrations.

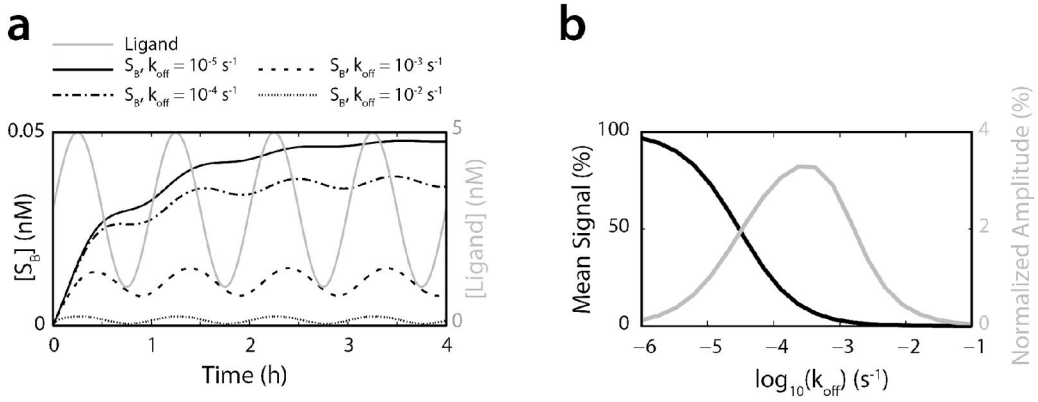

Figure 2.

A) Output profiles generated from an input varying from 1–5 nM with time period of 100 minutes. The output signals are read on the left vertical axis, the input signal is read on the right vertical axis shown in gray. B) Once the output oscillations are stabilized, the mean concentration and normalized amplitude are given as a function of k_{off}.

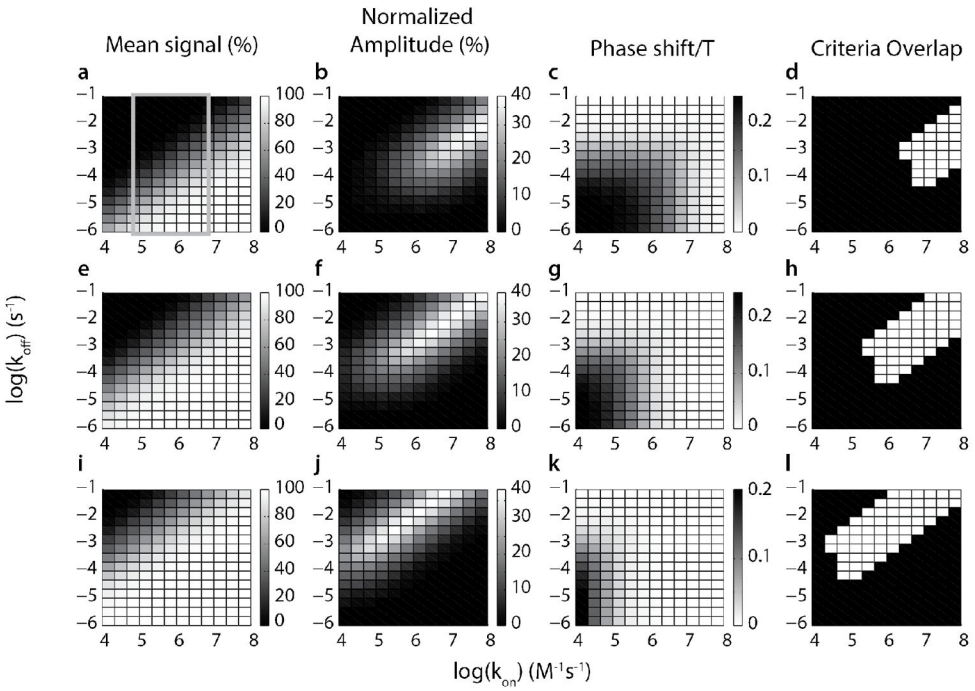

Figure 3.

Input signal of period of T = 100 minutes varying from 0.1–0.5 nM (top row), 1–5 nM (middle row), 10–50 nM (bottom row). The first column represents the mean signal as a percentage of the total sensor, the second column shows the normalized amplitude, the third column the phase delay and finally the last column is an overlap of the optimal regions for all three criteria. The areas accessible to engineering are shown in the gray box.

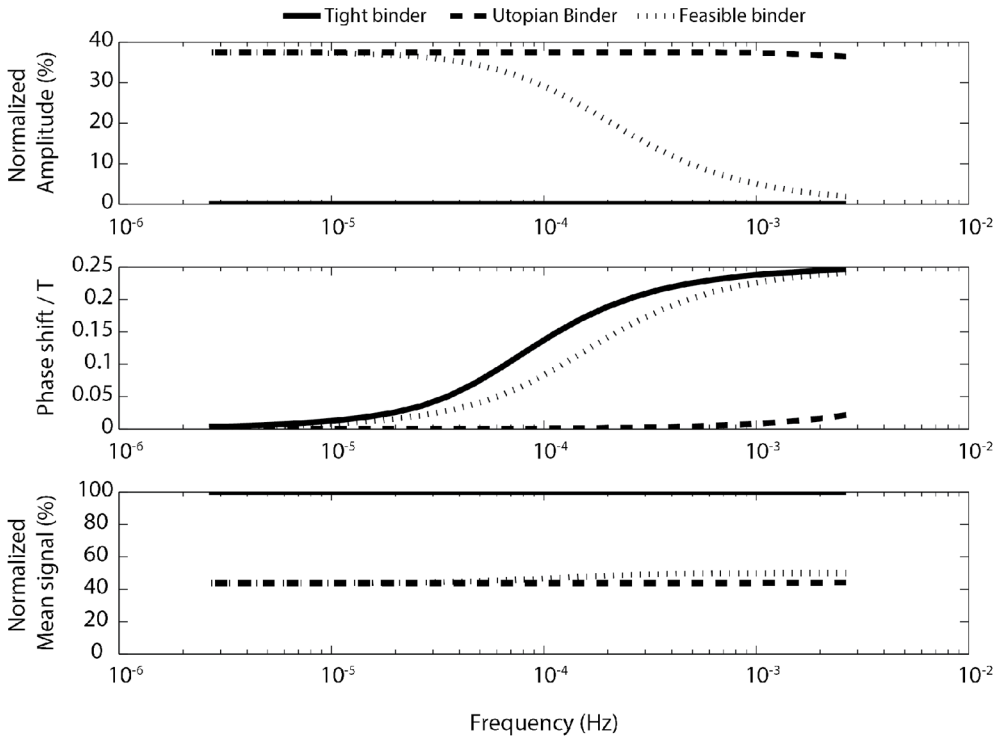

Figure 4.

Bode Diagram for three different sensors: In solid black we have represented a tight binder (k_{on} =10^6 $M^{-1}s^{-1}$, k_{off} = 10^{-6} s^{-1}), in dashed black a utopian binder given our model (k_{on} =10^8 $M^{-1}s^{-1}$, k_{off} = $3*10^{-1}s^{-1}$) and in dotted black a feasible binder (k_{on} =10^6 $M^{-1}s^{-1}$, k_{off} = $3*10^{-3}$ s^{-1}). The input signal varies between 1–5 nM and the sensor concentration is 0.05nM for all cases.

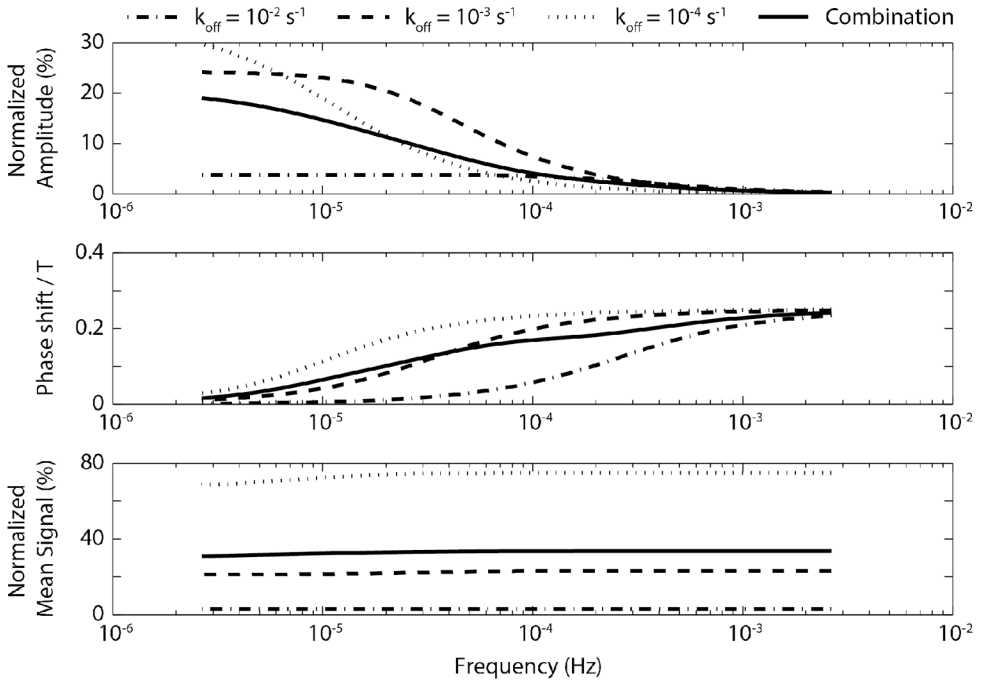

Figure 5.

Bode Diagram for individual and combinatorial sensor deployment. The input signal varies from 1–5nM, in all cases the total concentration of sensor(s) is equal to 0.05nM. All sensors have a k_{on} of $10^5 M^{-1}s^{-1}$.

Table 1

Optimum Location

Summary of the effect of input modification on optimum <k_{on}, k_{off}> couples. NE = No Effect

Input Property	Output Mean Signal	Output Normalized Amplitude	Output Phase Shift
Increasing Frequency	NE	$k_{on}\nearrow$ and/or $k_{off}\nearrow$	$k_{on}\nearrow$ and $k_{off}\nearrow$
Increasing Amplitude	NE	NE	NE
Increasing Mean	$k_{on}\nearrow$ and/or $k_{off}\searrow$	$k_{on}\searrow$ and $k_{off}\nearrow$	$k_{on}\searrow$ and $k_{off}\nearrow$